EPSC2017

SB9 abstracts

EPSC Abstracts
Vol. 11, EPSC2017-145-1, 2017
European Planetary Science Congress 2017

Deriving global Olivine distribution on Hayabusa's target (25143) Itokawa using Near-Infrared Spectrometer data

L. Nardi (1-2), E. Palomba (1), A. Longobardo (1), A. Galiano (1-3), F. Dirri (1)

(1) INAF-IAPS, Rome, Italy, (2) Università degli Studi di Roma La Sapienza, Rome, Italy, (3) Università degli Studi di Roma Tor Vergata, Rome, Italy

Abstract

In 2005 Hayabusa spacecraft visited asteroid Itokawa, bringing back surface samples to Earth in 2010. Near-Infrared spectra acquired by NIRS and samples analysis confirmed hypothesis made through ground-based observations, in particular the one that sees Itokawa as an LL-chondrite like asteroid processed by space weathering. In this work, we apply spectral indices for olivine detection on NIRS data. In particular, we define the BAR* and relate it to the olivine abundance, by means of calibration on laboratory data.

1. Introduction

Hayabusa was a JAXA spacecraft mission aimed at exploring the near-Earth asteroid (25143) Itokawa and bringing back surface samples. The spacecraft was equipped with four main scientific instruments:

1. Light Detection And Ranging instrument (LIDAR)
2. Asteroid Multi-band Imaging Camera (AMICA)
3. X-ray Fluorescence Spectrometer (XRS)
4. Near Infra-Red Spectrometer (NIRS)

Here we consider data from NIRS, which mapped the surface in the effective spectral range 850-2100 nm, where main olivine and pyroxene absorption features are partially visible. Between September and November 2005, NIRS took thousands of near-infrared spectra with a footprint within 6 and 90 m^2 and solar phase angle within 0° and 38°. Ground-based observations [3][5] have found out that Itokawa has an LL chondrite-like average composition with a sensible reddening due to space weathering effects. Subsequent samples analysis [9][11] confirmed these hypothesis, narrowing the classification range of analogs to LL4-LL6 ordinary chondrites [12].
First results from NIRS data [1] found a similarity between NIRS spectrum and Alta'ameem LL5 [8] spectrum measured by RELAB with a grain size of 125 µm. The 2 µm band centre, which is related to pyroxenes, is slightly different from Alta'ameem, suggesting some difference in mineralogical composition.
[4] used chondrites spectral data from [6] to evaluate Fa and Fs abundances on Itokawa's surface. They analyzed nearly 1600 spectra, obtaining Fa values between 25 and 30, and Fs values between 21 and 25, consistently with LL-like composition.

2. Methods

Since the NIRS spectral range does not cover entirely the two olivine and pyroxene bands, centered at ~1 µm and ~2 µm, we have to define suitable spectral parameters for retrieval of olivine. Band Area Ratio (BAR), which is defined as the ratio between the two band areas, is a good diagnostic for olivine detection [10], but is not really suitable here, since the two bands are not entirely covered by the NIRS spectral range. This issue could be avoided if the two bands were symmetric, but this is not the case, since olivine band at 1 µm is strongly asymmetric. The same problem exists at defining a band center at 1 µm, because it has to be calculated after continuum removal.
The BAR* parameter could be fundamental in this analysis because it regards just half band, from band shoulder to band minimum. The data used are the ones calibrated from [2]. These data are not photometrically corrected, but since BAR* is independent from illumination condition [7] we could avoid this passage. We have defined the band shoulder as the wavelength related to the maximum reflectance value between the two bands; then, half-band area is calculated as the area between a straight horizontal line with maximum value and the spectral curve, considered between its shoulder and its band minimum. We can use RELAB data of binary (olivine + low calcium pyroxenes) and ternary (olivine + low calcium pyroxenes + high calcium pyroxenes) mixtures to evaluate a relation between BAR* and olvine distribution; the next step is to apply this relation to NIRS data of Itokawa, in order to map the olivine distribution.

3. Preliminary results

In Figure 1 we show the distribution of BAR* calculated for nearly 38.000 spectra acquired from an altitude of ~3.5-7 km, defined as Home Position, which was the longest mission observation phase.
In Figure 2 a plot of olivine normalized content versus BAR* for RELAB compounds is given. Olivine normalized content is defined as

$$\widetilde{Ol} = \frac{Ol}{(Ol + Px)}$$

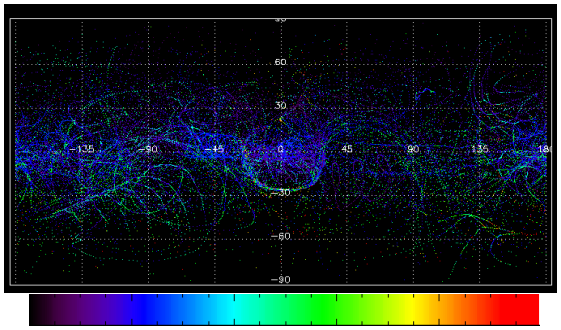

Figure 1: distribution of BAR from Home Position NIRS spectra. Blue is the lowest value, near 0.4, while red is the highest value, near 1.*

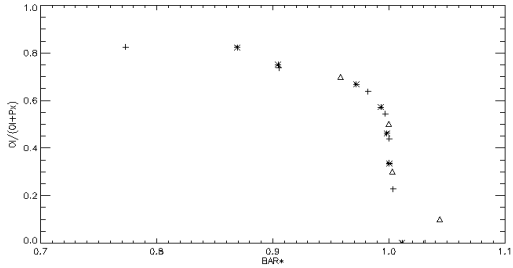

Figure 2: Olivine normalized content versus BAR as calculated in this work. Triangles indicates binary RELAB compounds, which are composed by olivine and low calcium pyroxenes. Crosses and stars indicates the two ternary mixtures, which are composed by olivine, low-calcium pyroxenes (LCP) and high-calcium pyroxenes (HCP). The difference is in the LCP/HCP ratio, which is 6 for LCP ternary mixtures (stars) and 1 for HCP ternary mixtures (crosses).*

4. References

[1] Abe M. et al. (2006), Science vol 312, 1334-1338.
[2] Abe M. et al. (2011), Hayabusa NIRS Calibrated Spectra V1.0. HAY-A-NIRS-3-NIRSCAL-V1.0. NASA Planetary Data System.
[3] Abell P.A. et al. (2007), Meteoritics & Planetary Science 42, Nr 12, 2165-2177.
[4] Bhatt M. et al. (2015), Icarus 262, 124-130.
[5] Binzel R.P. et al. (2001b), Meteoritics & Planetary Science, 36, 1167-1172.
[6] Dunn T.L. et al. (2010), Icarus 208, 789-797.
[7] Longobardo A. et al. (2014), Icarus, 20-35.
[8] Graham A.L. et al. (1978), Meteoritical Bulletin, no. 55, Meteoritics 13, 327-352
[9] Noguchi T. et al. (2011), Science vol 333, 1121-1124.
[10] Palomba E. et al. (2015), Icarus 258, 120–134.
[11] Thompson M.S. et al. (2014), Earth, Planets and Space, 66:89.
[12] Yurimoto H. et al. (2011), Science 333, 1116-1119.

EPSC Abstracts
Vol. 11, EPSC2017-166-1, 2017
European Planetary Science Congress 2017

On the impact of particle size on the characteristics of specular and diffuse reflectance spectra

U. Mall (1), B. Schmidt (2), B. Dabrowski (1), L. Hoenicke (1,2), D. Kloskowski (1,2),

(1) Max-Planck-Institut für Sonnensystemforschung, Justus-von-Liebig-Weg 3, 37077 Göttingen, Germany. (2) Institut für Mineralogie, GZG, Universität Göttingen, Goldschmidtstr. 1, Göttingen, Germany

Abstract

Reflectance spectra measurements of materials for studies related to their composition are routinely being made. The remote identification of minerals or rocks by reflectance measurements makes use of the fact that reflectance spectra in the UV-VIS-NIR and thermal infrared (TIR) wavelength regions of minerals contain a number of diagnostic features. These features arise by two different processes which can lead to either maxima or minima in the observed reflectance spectra: Surface scattering, which results from light that has been reflected from the surface without penetration and usually generate upward-going peaks in the reflectance spectrum and volume scattering which generates rays that have penetrated into the sample where the photons have been either scattered and absorbed thus leading to absorption minima. The detailed shape of these features depends on the various chemical and physical parameters of the illuminated sample material. A quantitative composition analysis of a mineral sample depends critically on how accurately one knows these dependencies and the effects of the parameters on the spectral characteristics (e.g. [3]). With the improved instrumentation flown on many recent space missions –resulting in spectra with higher spectral resolution – a better knowledge of the influence of the physical parameters become more important. Among the various physical parameters shaping a reflectance spectrum particle size has been known early on to play an important role (e.g., [1]) and to have a strong effect on albedo and absorption strength ([2]). For studies related to the mineral composition of planetary surfaces where one deals often with soils the analysis of these spectra turns out to be difficult. The analysis of regolith samples is particular complex because such samples are mixtures of different constituents, which can vary in all their characterizing parameters (see e.g. [6]). As regolith on exosphere bound surfaces is principally produced by meteoritic bombardment of the surface, its properties are products of several complex processes (see eg. [5]). Regolith soils such as those collected from the lunar surface contain a distribution of particle sizes that vary largely as a function of surface maturity (e.g. [6]). Many laboratory studies have been made to simulate regolith samples by mixing components of known minerals using specific grain size fractions. Often fraction as <45, 45–250, and 250–1000 µm are chosen. Some fractions have originally been chosen specifically to maximize the overall spectral contrast so that variations in absorption characteristics are well expressed (e.g. [2]). We are reporting on the characteristics of NIR measurements of pure minerals of well-defined grain sizes relevant for remote sensing studies of soils in specular and diffuse reflectance.

References

[1] Aronson, J.,R., Emslie, A.G. and Mc Linden, H.G., Infrared Spectra from Fine Particulate Surfaces, Science, 152, pp. 345-346, 1966.

[2] Crown, D. A., and C. M. Pieters, Spectral properties of plagioclase and pyroxene mixtures and the interpretation of lunar soil spectra, Icarus, 72, 492-506, 1987.

[3] Mall, U. et al., Towards A Quantitative Determination Of The Modal Mineralogy Of Planetary Surfaces Using Near-Infrared Spectroscopic Data From The Moon. LPSC XXXXIII, abstract #1893, 2012.

[4] McKay D.S, Fruland, R.M., and Heiken, G.H, Grain size and the evolution of lunar soils, LPSC, 5th, p. 887-906, 1974.

[5] McKay D.S, et al., The lunar regolith. In: Heiken GH, Vaniman DT, French BM (eds) Lunar sourcebook, pp. 284–356, Cambridge University Press, Cambridge, New York, Melbourne, 1991.

[6] Rommel, D. et al., Automatic Endmember Selection and Nonlinear Spectral Unmixing of Lunar Analog Minerals. ICARUS, 284, pp. 126-149, 2017.

EPSC Abstracts
Vol. 11, EPSC2017-435, 2017
European Planetary Science Congress 2017

A photometric survey of Near-Earth Objects in support of the NEOShield-2 project.

S. Ieva (1), E. Dotto (1), E. Mazzotta Epifani (1), D. Perna (1,2), M. A. Barucci (2), A. Di Paola (1), M. Micheli (1,3), E. Perozzi (4), R. Speziali (1), M. Lazzarin (5), I. Bertini (5), A. Giunta (1), D. Lazzaro (6), P. Arcoverde (6)
(1) INAF – Osservatorio Astronomico di Roma, Via Frascati 33, 00078 Monte Porzio Catone (Roma), Italy
(2) LESIA, Observatoire de Paris, PSL Research University, CNRS, Univ. Paris Diderot, Sorbonne Paris Cité, UPMC Univ., Paris 06, Sorbonne Université, 5 Place J. Janssen, Meudon Cedex F-92195, France
(3) ESA SSA-NEO Coordination Centre, Frascati, Roma, Italy
(4) Agenzia Spaziale Italiana - ASI, Via del Politecnico, snc, 00133 Roma, Italy
(5) Department of Physics and Astronomy 'Galileo Galilei', University of Padova, Vicolo dell'Osservatorio 3, I-35122 Padova, Italy
(6) Observatório Nacional, R. Gal. José Cristino 77, 20921-400 Rio de Janeiro, Brazil

Abstract

More than 85% of the 16,000 NEOs discovered up to now lack a physical characterization. The study of their physical properties is essential to define a proper mitigation scenario. One of the main aims of the NEOShield-2 project (2015-2017), financed by the European Community in the framework of the Horizon 2020 program, is therefore to retrieve physical properties of a wide number of NEOs, in order to design impact mitigation missions and assess the consequences of an impact on Earth.

1. Introduction

There is an urgent need to undertake a comprehensive characterization of the Near-Earth Object (NEO) population, due to the fact that these objects are crucial to put important constraints on the models of formation and evolution of our Solar System, and they could be responsible for the delivery of water and organics on early Earth [1]. Other than favouring life, NEOs can pose a serious hazard on human civilization. More than 16,000 NEOs are known nowadays. However, only less than 15% of them are physically characterized [2]. The lack of physical characterization is even more uncanny going to smaller objects (D < 300 m), since these bodies are the ones with a higher likelihood of catastrophic impact with the Earth. Moreover, NEOs show a great variation in terms of all mitigation-relevant quantities (size, shape, rotational period, composition, internal structure). The only way to proper design a future mitigation mission is therefore to obtain the physical properties for a wide number of NEOs.

The NEOShield-2 project (2015-2017) has been approved and financed by the European Commission in the framework of the Horizon 2020 program with the aims i) to study detailed technologies and instruments to conduct close approach missions to NEOs or to undertake mitigation demonstration, and ii) to retrieve physical properties of a wide number of NEOs, in order to design impact mitigation missions and assess the consequences of an impact on Earth.

In particular, the Italian team has been responsible for the Task 10.2.1 **'Colours and Phase function'**, with the aim to acquire photometric measurements of several NEOs in order to:

- perform a preliminary taxonomic classification using computed color indexes and obtain the first constraints on their surface composition and albedo;
- study the phase function to derive their H-G1-G2 parameters and have independent constraints on the taxonomic composition.

2. Results

We will present the results obtained at the Telescopio Nazionale Galileo (TNG, La Palma, Spain), during a 2-year Long-Term Program (September 2015 – September 2017), in which we carried out BVRI photometry of ~150 high profile NEOs, together with the phase functions we characterized using the Campo Imperatore telescope (L'Aquila, Italy) and the Observatório Astronômico do Sertão de Itaparica (Nova Itacuruba, Brazil). Targets were chosen among the ones with no physical characterization and preferentially with H > 20, which correspond, assuming a mean albedo, to objects with a diameter

D < 300 m. Using these data, we obtained color indexes and phase functions and we were able to derive visible color indexes and a preliminary taxonomic classification for each target in our sample. Then, we analyzed our sample according to their orbital parameters and their estimated size.

Acknowledgements

We acknowledged the support from the European Commission - grant agreement no: 640351 H2020-PROTEC-2014 - Access technologies and characterisation for Near Earth Objects (NEOs).

References

[1] Izidoro, A., de Souza Torres, K., Winter, O. C., Haghighipour, N., ApJ, 767, 54, 2013.

[2] https://www.earn.dlr.de/nea/table1_new.html

EPSC Abstracts
Vol. 11, EPSC2017-443-1, 2017
European Planetary Science Congress 2017

The Geminid Meteor Shower as observed by the CILBO Double Station Network

J. Zender (1), R. Rudawska (1) and D. Koschny (1,2)
(1) European Space Agency, ESTEC, Noordwijk, The Netherlands (2) Chair of astronautics, TU Munich, Germany

Abstract

We report on the current status of the processing, calibration, and analysis of spectral video data obtained from the Geminid meteor showers from 2011 until 2016. The spectral video data were acquired by the Canary Island Long-Baseline Observatory (CILBO), that also provides double station videos, allowing to compute the orbit for individual meteors.

1. Introduction

The Meteor Research Group (MRG) of the European Space Agency operates double station, called CILBO (Canary Island Long-Baseline Observatory). Currently, five image-intensified video cameras observe the night sky every clear night. The system is sensitive to sporadics and shower activity. Since full operations in 2012, about 70000 meteors have been observed. With two of the cameras (ICC7 and ICC9), we have recorded almost 20000 double-station meteors, while recently installed large field-of-view cameras (LIC1 and LIC2) typically record between 1300 and 1700 meteors per month. For detailed information about CILBO and its setup, please see [2]. The 3D trajectory and heliocentric orbits of these meteoroids were computed, and stored in the Virtual Meteor Observatory (VMO), which is the long-term archive of the International Meteor Organisation's video meteor camera network. In particular, it contains a record of precise measurements of Geminid meteors. The Geminids meteor shower, thought to originate from dust emitted by 3200 Phaethon, show a complicated structure, including a double-peaked activity profile [1]. In 2009, weak activity of asteroid Phaethon itself was reported, [1] and [3]. The most plausible reason behind the observed brightening is the dust production by thermal fracture and decomposition [4]. The abundance of sodium in Geminid shower dust particles vary strongly and in most spectra, Sodium is abundant [7].

2. Data Analysis

For the period from 2010 onwards, the cameras have recorded 20 events in all three cameras: ICC7, ICC9, and the spectral camera ICC8. We recalculated the orbital elements from the double station observation information and confirm the known Phaeton (2013) orbital elements.

The 3D plot, shown for the Geminids observed in 2011 in Figure 1, shows several substructures within the stream, filaments, that could indicate different ejection times of the dust particles.

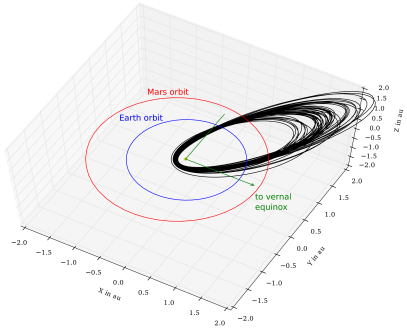

Figure 1: Computed orbits for Geminid meteors in 2011.

Figure 2 plots the semimajor axis (a) against eccentricity (e) of individual meteor events. It thus shows the evolution of the orbital elements against. Larger meteoroid masses are indicated by larger point areas in the plot. The orbital propagation was computed using the RADAU integrator in the MERCURY software and is solely based on gravitational effects.

Figures 3 and 4 show the spectral response of two Geminid events of 2013. Figure 3 is showing a high sodium content in the meteor, that is rarely observed in Geminid meteor spectra, see [5], [6] and [7].

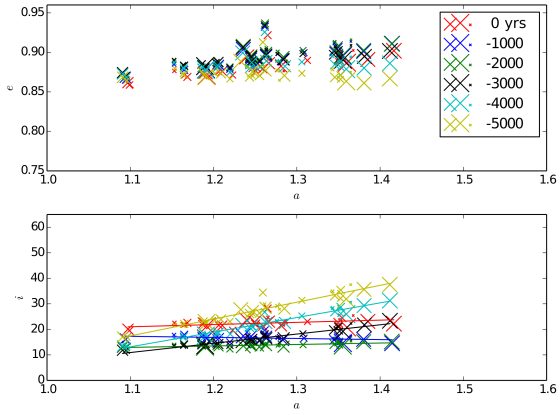

Figure 2: Orbital elements of individual Geminid meteor shower events.

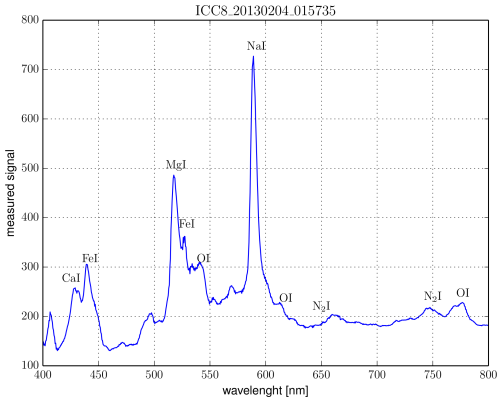

Figure 3: Calibrated spectrum of Geminid spectra 20130204T015735.

3. Summary

We present a snapshot of the ongoing analysis of the Geminid meteor shower data obtained by the Canary Island Long-Baseline Observatory (CILBO) of the ESA's Meteor Research Group (MRG). The analysis includes the determination of individual orbital elements and the propagation of these. Spectral data are calibrated and analyzed in view of abundances of the main chemical elements of meteoritic spectra.

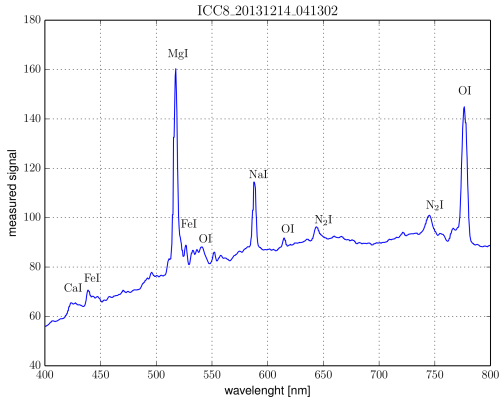

Figure 4: Calibrated spectrum of Geminid spectra 20131214T041302.

Acknowledgements

The authors would like to thank the Faculty of ESA's Science Support Office for the continuous support on the CILBO Project.

References

[1] Jewitt, D. and Li, J.: The dust tail of asteroid (3200) Phaethon, 2010, AJ, 140, 1519

[2] Koschny, D. et al.: A double-station meteor camera set-up in the Canary Islands - CILBO Geosci. Instrum. Method. Data Syst., 2, 339, 2013

[3] Li, J. and Jewitt, D.: Recurrent Perihelion Activity in (3200) Phaethon AJ, Volume 145, Issue 6, article id. 154, 9 pp. (2013).

[4] Ryabova, G.: A preliminary numerical model of the Geminid meteoroid stream MNRAS, Volume 456, Issue 1, p.78-84

[5] Borovička, J. et al: Spectral, Photometric, and Dynamic Analysis of Eight Draconid Meteors, Earth, Moon, and Planets, October 2014, Volume 113, Issue 1, pp 15–31

[6] Rudawska, R. et al: Birth of meteor network in Morocco – Analysis for the 2012 Geminids WGN, the Journal of the IMO 41:4, 2013

[7] Čapek, D. and Borovička, J.: Quantitative model of the release of sodium from meteoroids in the vicinity of the Sun: Application to Geminids Icarus 202 (2009) 361–370

EPSC Abstracts
Vol. 11, EPSC2017-516-1, 2017
European Planetary Science Congress 2017

Bias on the “average” photometric behaviour

F. Schmidt (1), S. Bourguignon (2)
(1) GEOPS, Univ. Paris-Sud, CNRS, Université Paris-Saclay, Rue du Belvédère, Bât. 504-509, 91405 Orsay, France (2) Laboratoire des Sciences du Numérique de Nantes, École Centrale de Nantes, France (frederic.schmidt@@u-psud.fr)

Abstract

The Hapke model has been widely used to describe the photometrical behaviour (reflectance as a function of incidence and emergence direction) of planetary surface but the uncertainties of retrieved parameters has been difficult to handle so far. A recent study proposed to estimate the uncertainties using the Bayesian approach [1]. Here, we propose an improvement of the numerical implementation to speed up the uncertainties estimation. We study the common analysis scheme to summarize a collection of data from various locations in order to answer the question: are these locations photometrically homogeneous or not? For instance, this question arises when combining data from an entire planetary body, each pixel with a single *angel* (angular sampling noted *angel*). We tested here the ability of the Bayesian method to decipher two situations, in the presence of noise: (i) a photometrically homogeneous surface (all pixel with the same behaviour), (ii) an heterogeneous surface with 2 distinct photometrical properties (half pixels with behaviour A, other half with behaviour B). The results suggests that the Bayes method is able to distinguish the two situation and thus, to have access to an information about the photometric heterogeneities of a body.

1. Introduction

The Bi-directional Reflectance Distribution Function (BRDF) is the core quantity to describe the photometric behaviour [2]. It represents the same location pixel (for picture element), observed with various angular element (angel, for angular element) [3]. Hapke proposed a semi-analytical model of the BRDF of a granular medium [2]. Many authors have been using it to analyze laboratory data [4, 5], telescopic observation [6], in situ data [7], remote sensing data [8] due to its relative simplicity and fast computation. Following our previous study [1], we not to discuss the realism of the photometric Hapke model, but focus on the data analysis point of view in order to distinguishing homogeneous versus heterogeneous photometric dataset.

2. Method

We performed a synthetic test in order to better understand the behaviour of the bayesian analysis in the case of heterogeneous dataset. We generate 100 geometrical configurations randomly with a uniform distribution in an half space in order to define the angels. We then compute the direct Hapke model to create 100 synthetic observations. We propose to consider a noise level of 10% as a upper but realistic bound in this study. We split the 100 angels randomly in two. We attribute the first half with one set of Hapke photometric parameters, namely same single scattering albedo ω, roughness angle θ, particle phase function parameters b/c [2]. The other half is attributed to another set of Hapke parameter. This way, we generate a dataset of heterogeneous photometric behaviour (see fig. 1).

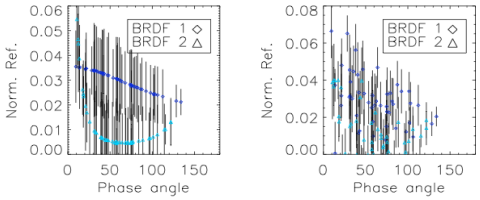

Figure 1: Input data for the synthetic test: normalized reflectance for 100 observations in a random geometry. Hapke parameter are the same ω=0.1, θ=0.5°. Dark blue: 50 samples (BRF1) with broad backward scattering (b=0.1, c=1.0), Light blue: 50 samples (BRF2) with narrow forward scattering (b=0.8, c=0.1). Left: without noise. Right: with 10% level of noise.

We decide to study one parameter change only, for instance the particle phase function in figure 1, and two choose extreme conditions for this parameter. As

an example, in figure 1 shows broad backward scattering and narrow forward scattering. One can note that the two dataset are clearly separated when there is no noise. When adding noise, it is impossible by eyes to distinguish both datasets. All the game is now to retrieve the Hapke parameters in this heterogeneous configuration that could occur in real dataset, when the observation are not collected at the same time and same location of the surface.

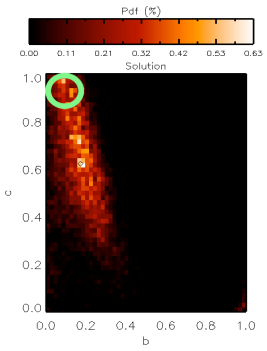

Figure 2: Results of the estimation of b and c parameters for 50 observation of BRF1 only. (green circle represent the true solution without noise)

3. Results and discussion

Figure 2, 3 and 4 represent the results of the Monte Carlo Bayesian analysis. If we consider only 50 angels of a homogeneous surface (figure 2 and 4), the retrieval method is consistent with the known photometric parameters. Please note that the exact value is not perfectly retrieved simply because of the tolerance due to noise. In the case of 100 angels in a heterogeneous surface (figure 3), the solution is not two maxima near the two true solutions, as one may expect, but an intermediate fake solution. Thus, the Bayesian solution (and obviously all other methods estimating the minimum chi-square solution) seems to be cheated by an heterogeneous dataset.

Nevertheless, an in-depth study of the best solution (minimum chi-square) reveals that only the homogeneous case is compatible with input noise level at a confidence level of 95%. This test fails for the heterogeneous case. Thus, we propose a new approach to distinguish heterogeneous datasets from homogeneous ones, by first using the bayesian approach to minimize the chi-square without being perturbed by local minima, and then to analyze the confidence of the best solution [9]. This strategy should now be applied in real datasets.

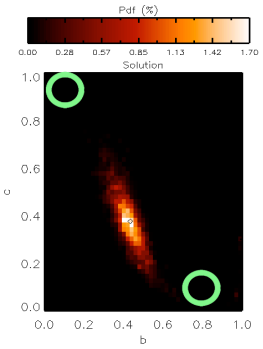

Figure 3: Idem fig. 2 but for 100 observation of BRF1 and BRF2.

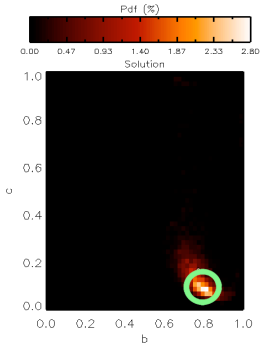

Figure 4: Idem fig. 2 but for 50 observation of BRF2.

References

[1] Schmidt et al. (2015), Icarus, 260, 73 - 93 [2] Hapke, B. (1993), Cambridge UP. ., book [3] Andrieu, F. et al. (2016), The Cryosphere, 2113-2128. [4] Cord, A. et al., (2003), Icarus, 414-427. [5] Johnson, J., (2013), Icarus 383-406. [6] Hapke, Icarus (1998), 89-97. [7] Johnson, J., J. Geophys. Res. (2006), E12S16 [8] Fernando J. et al, (2016), Icarus, 28, 30-51 [9] Schmidt., F. et al. (2017), Icarus, under review

EPSC Abstracts
Vol. 11, EPSC2017-704, 2017
European Planetary Science Congress 2017

Continuum definition for Ceres absorption bands at 3.1, 3.4 and 4.0 µm

A. Galiano (1,2), E. Palomba (1), A. Longobardo (1), A. Zinzi (3,4), M.C. De Sanctis (1), A. Raponi (1), F.G. Carrozzo (1), M. Ciarniello (1), F. Dirri (1)
(1) INAF-IAPS, Rome, Italy (anna.galiano@iaps.inaf.it), (2) Università degli Studi di Roma Tor Vergata, Rome, Italy, (3)ASI Science Data Center, (4) INAF-OAR.

Abstract

The images and hyperspectral data acquired during various Dawn mission phases (e.g. Survey, HAMO and LAMO) allowed identifying regions of different albedo on Ceres surface, where absorption bands located at 3.4 and 4.0 µm can assume different shapes. The 3.1 µm feature is observed on the entire Ceres surface except on *Cerealia Facula*, the brightest spot located on the dome of Occator crater [1]. To perform a mineralogical investigation, absorption bands in reflectance spectra should be properly isolated by removing spectral continuum; hence, parameters as band centers and band depths must be estimated. The problem in the defining the continuum is in the VIR spectral range, which ends at 5.1 µm even though the reliable data, where the thermal contribution is properly removed, stops at 4.2 µm [2]. Band shoulders located at longer wavelengths cannot be estimated. We defined different continua, with the aim to find the most appropriate to isolate the three spectral bands, whatever the region and the spatial resolution of hyperspectral images [3]. The linear continuum seems to be the most suitable definition for our goals. Then, we performed an error evaluation on band depths and band centers introduced by this continuum definition.

1. Introduction

Since March 2015, the *Visible-Infrared Imaging Spectrometer*-VIR [3] and the *Framing Camera*-FC [4] acquired Ceres hyperspectral data and images with increasing resolution, by several mapping orbits performed by NASA Dawn spacecraft (i.e. Survey, HAMO and LAMO phases). Spectrally, the Ceres average surface exhibits absorption bands at about 2.7, 3.1, 3.4 and 4.0 µm, ascribed to phyllosilicates, ammoniated, Calcium- and/or Magnesium-carbonates, respectively [5]. Regions of different equigonal albedo are detected, where the 3.1, 3.4 and 4.0 µm bands can assume slightly dissimilar shapes. Bright areas or bright spots (BS) were identified widespread on Ceres surface: the brightest spot, *Cerealia Facula*, lies on the dome of Occator crater. It is minerally composed by Aluminum-phyllosilicates and high abundance of Sodium-carbonates, as inferred for the longward shift of the 2.7 µm band, the lack of 3.1 µm feature and the strong carbonate absorptions at 3.4 and 4.0 µm. Due to the absence of 3.1 µm band, the left shoulder of 3.4 µm feature is located at shorter wavelengths than the mean Ceres spectrum [1]. To compare parameters of spectra acquired in several phases of mission and from areas with unlike albedo, the same continuum removal method should be applied on the whole VIR dataset. VIR spectral range spans from 0.25 to 5.1 µm, but the reliable and thermally corrected data ends at 4.2 µm [2], making difficult the identification of band shoulders at longer wavelengths. We defined three types of continua (a linear continuum and two that make use of polynomial curves), selecting the one best suited to describe spectra of various regions and properly isolate the 3.1, 3.4 and 4.0 µm absorption bands. Furthermore, for the first time, we estimated the errors on band depths and band centers: this is fundamental to compare spectral parameters of Ceres regions and perform mineralogical and photometric analyses.

2. Description of the method

The spectral continua of 3.1, 3.4 and 4.0 µm features were fitted by using three methods: a linear continuum, a 3rd order polynomial curve (Continuum 1) and a 2nd order polynomial curve (Continuum 2). The linear continuum involves three straight lines, with the endpoints calculated on the shoulders of bands. The left and right shoulders of 3.1 µm band were fitted by a 2nd order polynomial curve in the 2.8-3.0 µm and in the 3.16-3.27 µm range, respectively. The wavelengths corresponding to the maximum fitted value were selected as continuum boundaries. For the 3.4 µm band, the wavelengths corresponding

to local maxima of reflectance level in the 3.05-3.36 µm and in the 3.55-3.68 µm range, respectively, were detected. The boundaries of 4.0 µm band were selected in the ranges 3.55-3.68 µm and 4.05-4.15 µm, respectively. The Continuum 1 was produced by forcing the passage for four local maxima, evaluated in four ranges: 2.85-3.0 µm (R1); 3.17-3.25 µm (R2); 3.65-3.69 µm (R3); 4.0-4.3 µm (R4). The Continuum 2 passes for three local maxima, estimated in the R1, R3 and R4. We applied methods on smoothed spectra acquired during the Survey (altitude 4400 km and spatial resolution ~1.1 km/pixel), HAMO (altitude 1470 km and spatial resolution 360-400 m/pixel) and LAMO (altitude 385 km and spatial resolution 90-110 m/pixel) phases. The selected spectra are representative of dark, intermediate and bright regions and of Cerealia Facula BS. The selection of regions has been performed basing on equigonal albedo values, estimated at 1.2 µm [6].

3. Application of the method

To calculate and compare spectral parameters, the same continuum must be fitted on spectra of any region and removed to properly isolate absorption bands. Continuum 1 properly fits spectra of dark, intermediate and bright regions. The curve is, however, high sensitive to the increasing reflectance over 3.5 µm and therefore, the fitted continuum can assume a slight convexity in the 3.1 and 3.4 µm band and a concavity in the 4.0 µm band. In Occator BS spectra, this effect is highlighted, compromising the correct isolation of bands and the evaluation of spectral parameters. The Continuum 2 is always a good fit for the 4.0 µm band, but it's inappropriate for 3.1 and 3.4 µm bands. The linear continuum can isolate the three absorption bands in any region and predict the lack of 3.1 µm feature in Occator BS spectra. The behavior of three methods on a HAMO spectrum of a bright region, is shown in Figure 1.

4. Error evaluations

A smoothing of reflectance is applied to spectra to reduce the signal fluctuations. The fitted continuum is then removed from the smoothed spectra so that band center and band depth are estimated. The smooth procedure can alter the spectrum and introduce error in the retrieved parameters. Therefore, we removed the fitted continuum from both smoothed and unsmoothed spectra and we estimated the variation of band centers and band depths as uncertainty on the retrieval. The maximum error for the 3.1 and 4.0 µm band centers is well below the VIR spectral resolution, therefore we can assume 0.005 µm as maximum variation, i.e. half the value of VIR spectral sampling. The error associated to the 3.4 µm band center is 2.2%. The highest relative percentage errors (considering dark, intermediate and bright regions) are 3%, 18% and 21% for the 3.1, 3.4 and 4.0 µm band depth, respectively. In Occator BS spectra, the smoothing application slightly change values of carbonates band depths (probably due to the high signal-to-noise ratio), with a maximum error of 2.2% and 1.6% for the 3.4 µm and 4.0 µm feature, respectively.

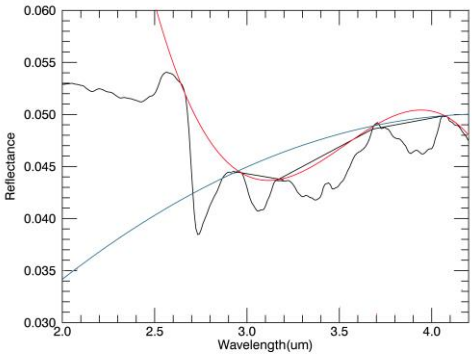

Figure 1: Linear continuum (black line), Continuum 1 (red line) and Continuum 2 (blue line) are superimposed on the spectrum of a bright region acquired in the HAMO phase.

References

[1] De Sanctis, M.C. et al.: Bright carbonate deposits as evidence of aqueous alteration on (1) Ceres, Nature, Vol. 536, pp. 54-57, 2016.

[2] Raponi, A. et al., submitted to Icarus, 2017.

[3] De Sanctis, M.C. et al.: The VIR spectrometer, Space Science Review, Vol. 163, Issue 1-4, pp. 329-369, 2011.

[4] Sierks, H. et al.: The Dawn Framing Camera, Space Science Review, Volume 163, Issue 1-4, pp. 263-327, 2011.

[5] De Sanctis, M.C. et al.: Ammoniated phyllosilicates with a likely outer Solar System origin on (1) Ceres, Nature, Vol. 528, pp. 241-244, 2015.

[6] Longobardo, A. et al.: EPSC Abstract, 2017.

EPSC Abstracts
Vol. 11, EPSC2017-743-1, 2017
European Planetary Science Congress 2017

Asteroid phase-curves from Gaia-calibrated data

D. Oszkiewicz (1), B. Skiff (2), B. Warner (3), M. Buie (4) P. Tanga (5) M. Popescu (6) , A. Cellino (7) , J. Licandro (8), D. Hestroffer (9)
(1) Institute Astronomical Observatory, Adam Mickiewicz University, Poznań, Poland (dagmara.oszkiewicz@astro.amu.edu.pl) (2) Lowell Observatory, USA (3) Center for Solar System Studies, USA (4) Southwest Research Institute, USA (5) Nice Observatory, France (6) Astronomical Institute of the Romanian Academy, Romania (7) INAF, Osservatorio Astronomico di Torino, Italy (8) Instituto Astrofisica de Canarias, Spain (9) IMCCE, Observatoire de Paris, PSL Research University, CNRS, Paris, France

Abstract

We use asteroid differential photometry gathered in the past decades together with the Gaia stellar catalogue (as photometric standards) to obtain relative magnitudes. The obtained magnitudes are then used to fit the multi-opposition phase curves in several ways depending on data quality.

1. Introduction

Modern CCD photometric observations of asteroids are traditionally done using differential photometry. That is only the differences between the asteroid and a comparison star are obtained without placing the measurements on a standard photometric system. Differential photometry has been used for decades and is sufficient for a variety of applications, like determining the rotational period, spin axis orientation and shape. It is however not very useful for determining asteroid absolute magnitudes and phase curve parameters, where relative magnitudes are required.

Obtaining relative photometry is typically avoided due to lack of photometric standards in the field of view and/or lack of photometric weather during observations. Thus not many accurately determined phase curves based on dense data (such as those in for example [1] [2]) are available (low accuracy phase curves are available for several hundreds of asteroids [3], [4]).

This problem can be completely solved with the Gaia mission catalogue. Gaia is a space observatory launched in 2013 by the European Space Agency [5] [6]. The ongoing mission is currently cataloging approximately 1 billion astronomical objects. The first catalogue (DR1) was released in 2016. Subsequent releases are planned in stages with the last, fifth (containing asteroid data) planned in 2022. Due to the number of stars, high photometric precision and accuracy, the stars measured by Gaia are suitable to use as photometric standards. Most of the historical CCD images contain Gaia photometric stars, making it possible to re-measure asteroid magnitudes from the images and by placing them on a standard photometric system obtain relative measurements.

2. Data

We have gathered a substantial 7.26 TB of possible data to use in the project. In Table 1 we summarize the data available for this project. The data secured stretch decades of observations (from 1992 until now) and contain multiple lightcurves for thousands of asteroids. Most photometric observations in our datasets were taken with a Cousins R filter, but some with Johnson V filter, Sloan r', or a wide-band VR filter. Data obtained at the RBT telescope are obtained mainly in the wide-band L (luminosity) filter. Some observations are done in so called Open filter (unfiltered) and those might be challenging to convert to relative photometry. However those constitute a small fraction of our entire dataset. It is possible to include further datasets if available during the course of the project.

Telescope	Aperture	Instrument	Institute
PTP	0.4m	SBIG	PO
RBT	0.8 m	SBIG	PO
various	various	various	CSSS
31-inch	0.8m	nasa31	LO
Hall	1.1m	nasa42	LO
Perkins	1.8m	prism	LO

Table 1: Telescope data available for this project. Abbreviations: PO- Institute Astronomical Observatory, Adam Mickiewicz University in Poznań, LO- Lowell Observatory, CSS - Center for Solar System Studies.

3. Relative magnitude calibration

We will perform standard photometric reductions with bias and flat-field correction followed by ordinary aperture photometry. We will use the Gaia catalogue to obtain the G nightly zero-points. The G magnitude relates to Sloan r' linearly: $r'_{Sloan} = G + 0.066$. We will use two or more comparison stars in each field, of much higher signal-to-noise than the target (when possible). When possible we will select the comparison stars to have near-asteroidal colors. For asteroids near their stationary points, we might be able to use the same comparison star sets on multiple nights. The measuring apertures will be adjusted depending on each image quality.

4. Phase curve fitting

For asteroids with data from a single opposition we will use the standard Fourier fitting to determine magnitude shifts between the different lightcurves. Those will then be directly used to fit phase curves and obtain absolute magnitudes. For multi-opposition data we can use two approaches. First for asteroids with limited data we would use approach similar to [3] where average aspect corrections were adopted. For sparse and low quality objects modified phase functions [9] will be used. For asteroids with larger amounts of data we will use more accurate brightness model, where apparent magnitude is given by [7]:

$$V(\alpha,\eta) = 5\log_{10}(r\Delta) + f(\alpha,H,G_1,G_2) + 2.5\log_{10}(\Delta S(P,\lambda_p,\beta_p,a/b,b/c,\phi_0)) \quad (1)$$

where r is the asteroid - Sun distance, Δ is the asteroid-Earth distance, α is the phase angle (Sun-Asteroid-Earth angle), and η denotes the vector of unknown parameters in the model $\eta = [P,\lambda_p,\beta_p,a/b,b/c,\phi_0,H,G_1,G_2]$. The parameters are: P - rotational period, (λ_p, β_p) - rotational pole coordinates, (a/b, b/c) - shape axis ratios, ϕ_0 - initial rotational phase, H is absolute magnitude and (G_1, G_2) are phase curve parameters. For the phase function $f(\alpha,H,G_1,G_2)$ we use H, G_1, G_2 function developed by [8] and adopted by the IAU in 2015.

5. Summary and Conclusions

The Gaia mission will provide data for asteroids at large phase angles. Due to small range of the phase angle covered the Gaia data on their own are insufficient to fit phase curves and calculate asteroid magnitudes. However the Gaia stellar catalogue can be used as a photometric standard catalogue. By combining the Gaia catalogue with the historical asteroid differential photometry we can derive relative magnitudes and fit thousands of asteroid phase curves.

Acknowledgements

This work is proposed within the DIAMOND collaboration network.

References

[1] Shevchenko, Vasilij G., et al. "Asteroid observations at low phase angles. IV. Average parameters for the new H, G 1, G 2 magnitude system." Planetary and Space Science 123 (2016): 101-116.

[2] Pravec, P., et al. "Absolute magnitudes of asteroids and a revision of asteroid albedo estimates from WISE thermal observations." Icarus 221.1 (2012): 365-387.

[3] Oszkiewicz, D.A., et al. "Online multi-parameter phase-curve fitting and application to a large corpus of asteroid photometric data." Journal of Quantitative Spectroscopy and Radiative Transfer 112.11 (2011): 1919-1929.

[4] Oszkiewicz, D.A., et al. "Asteroid taxonomic signatures from photometric phase curves." Icarus 219.1 (2012): 283-296.

[5] Prusti, T., et al. "The Gaia mission." Astronomy & Astrophysics 595 (2016): A1.

[6] Brown, A., et al. "Gaia Data Release 1-Summary of the astrometric, photometric, and survey properties." Astronomy & Astrophysics 595 (2016): A2.

[7] Wang, Y.-B., et al. "Study of photometric phase curve with new brightness model: refining phase function system parameters of asteroid (107) Camilla." Research in Astronomy and Astrophysics 16.9 (2016): 015.

[8] Muinonen, K., et al. "A three-parameter magnitude phase function for asteroids." Icarus 209.2 (2010): 542-555.

[9] Penttilä, A., et al. "H, G 1, G 2 photometric phase function extended to low-accuracy data." Planetary and Space Science 123 (2016): 117-125.

EPSC Abstracts
Vol. 11, EPSC2017-744, 2017
European Planetary Science Congress 2017

Radar observations of near-Earth Asteroids using the Quasar VLBI Network Telescopes

Yu. Bondarenko, Yu. Medvedev, D. Vavilov and D. Marshalov
Institute of Applied Astronomy of the Russian Academy of Sciences, Russia (bondarenko@iaaras.ru)

Abstract

We report results of intercontinental bistatic radar observations of near-Earth Asteroids 2011 UW158, 2003 YT1, 2014 JO25 and 2003 BD44 which have been carried out using the Goldstone and Quasar VLBI Network Telescopes for three years. Analysis of observations allowed us to estimate the size and spin period, which agrees with the photometric observations as well as obtain some information about asteroid's shape and near-surface roughness.

1. Introduction

Today, radar astronomy is one of the most effective techniques for determining the physical properties of near-Earth asteroids (NEAs). The size, shape, spin period and surface properties of NEAs can be obtained using radar observations. Since 2015 intercontinental radar observations are regularly carried out at the Institute of Applied Astronomy of the Russian Academy of Sciences in cooperation with the Goldstone Observatory using 70 m antenna (DSS-14) to transmit and 32 m radio telescopes (RT-32) of Quasar VLBI network in Svetloe, Zelenchukskaya and Badary observatories to receive the echoes [1]. Such type of radar observations called bistatic, where the transmitter and receiver are located on different antennas.

2. Observations

Usually the DSS-14 radar transmits a circularly polarized continuous wave (CW) signal at 8560 MHz (3.5 cm). We use two sets of separate channels at the RT-32 telescopes to receive echoes in the same (SC) and opposite (OC) circular polarizations as that of the transmitted wave. The received echo is sampled by R1002M Data Acquisition System and recorded by Mark5B [2]. Taking into account the Doppler frequency as a function of time we apply the Fourier transform to the echo time series. As a result we obtain CW echo power spectra for selected time intervals with the required frequency resolution. At the Fig. 1 you may see the example of such echo power spectra of 2001 UW158 near-Earth Asteroid. Echo power is plotted in standard deviations versus Doppler frequency relative to the estimated frequency of echoes from the asteroid's center of mass. Solid and dashed lines denote echo power in the OC and SC polarizations. Circular polarization of the signal is reversed after reflection from the plane surface and the maximum power of the reflected signal is expected in the OC polarization, though some of the signal, due to secondary reflections, is received with the same polarization. The ratio of SC to OC is a measure of near-surface wavelength-scale roughness [3].

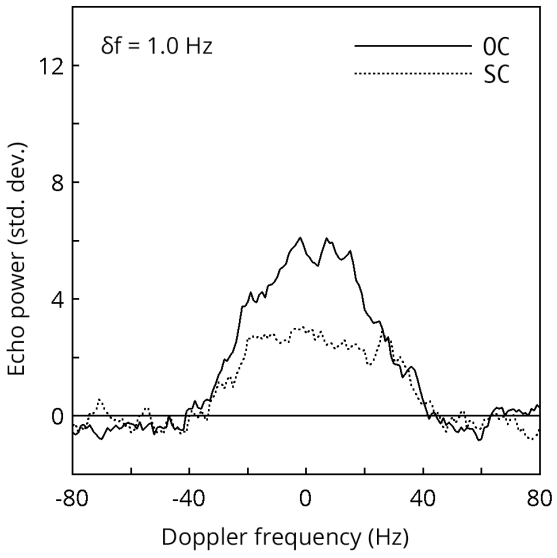

Figure 1: Opposite- and same-circularization continuous wave echo power spectra of 2011 UW158 obtained at Zelenchukskaya observatory.

3. Shape

The power spectrum bandwidth as function of time can be used for obtain the spin period in case of long observation series. Taking the geometric relation between echo power spectrum and the shape of rotating asteroid [4] into account, we estimate the hull of asteroids polar silhouette. Knowing the obtained spin period and assuming that the spectrum bandwidth is a continuous vector function of rotation phase we use least squares to fit an 3-harmonic Fourier series to the data vector. The result is a two-dimensional convex hull which is a projection of the asteroid onto its equatorial plane. To convert Hz to meters we assume that the asteroid-centered declination of the radar is equal to zero. Obtained convex hull of 2011 UW158 polar silhouette is shown in Fig. 2. The solid profile represents the joint solution and the dotted profiles correspond to the observatories individually. The Earth is toward the bottom of the Fig. 2. The figure shows that the body has an elongated shape with dimensions varies from 350 to 520 meters, which is consistent with the radar observations of the Arecibo, Green Bank and Goldstone observatories [5].

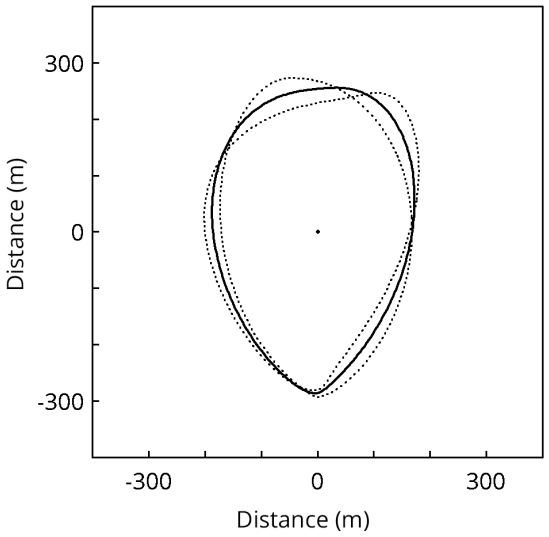

Figure 2: Convex hull of 2011 UW158 polar silhouette.

4. Summary

The radar echoes of signals transmitted from the 70 m antenna of the Goldstone Observatory were successfully detected. Obtained results confirm the possibility and effectiveness of the bistatic radar observations of near-Earth Asteroids using 32 m radio telescopes of Quasar VLBI network as receiving part of a bistatic configuration. It was shown that receiving and processing of the continuous wave echo allows to estimate the value of the Doppler frequency with sufficient accuracy which can be used to obtain the spin period and size of Near-Earth Object. Following this positive experience we plan to continue bistatic radar experiments for obtaining continuous wave spectra and range-Doppler images in the near future. This work was supported by the Russian Scientific Foundation grant No 16-12-00071.

References

[1] Ipatov, A., Bondarenko, Yu., Medvedev, Yu., Mishina, N., Marshalov, D., Benner L.: Radar observations of the asteroid 2011 UW158, Astromical Letters, Vol. 42, pp. 850-855, 2016.

[2] Grenkov, S., Nosov, E., Fedotov, L., Koltsov, N.: A Digital Radio Interferometric Data Acquisition System, Instruments and Experimental Techniques, Vol. 53, Iss. 5, pp. 675-681, 2010.

[3] Benner, L., Ostro, S., Magri, C., Nolan, M. at.al.: Near-Earth asteroid surface roughness depends on compositional class, Icarus, Vol. 198, pp. 294-304, 2008.

[4] Ostro, S., Rosema, K., and Jurgens, R.: The Shape of Eros, Icarus, Vol. 84, pp. 334-351, 1990.

[5] Naidu, S., Benner, L., Brozovic, M., et.al. Radar observations of near-Earth asteroid (436724) 2011 UW158 using the Arecibo, Goldstone, and Green Bank Telescopes, DPS meeting 47, Book of Abstracts, 2015.

EPSC Abstracts
Vol. 11, EPSC2017-790, 2017
European Planetary Science Congress 2017

Spectral analysis via comparison of band characteristics

S. Erard

LESIA, Observatoire de Paris, PSL Research University, CNRS, Sorbonne Universités, UPMC Univ. Paris 6, Univ. Paris Diderot, Sorbonne Paris Cité, France (stephane.erard@obspm.fr)

Introduction

Study of the composition of planetary surfaces relies intensively on spectral observations and comparisons with laboratory data. However, spectroscopy data can be particularly difficult to compare because they consist in very correlated data sets where the relevant information only bears a small fraction of the overall variance. To go beyond the usual process of manually selecting samples and fitting spectra, both band extraction techniques and band lists of laboratory spectra must be available to support automated identification of spectral signatures.

Building on the Mulțumesc algorithm [1], the procedure presented here is an assessment of spectral matching based on band characteristics only, rather than fit of complete reflectance spectra. This procedure is expected to remove dependency on the spectral continuum and focus entirely on band location and shape, which carry the main compositional information.

Spectral fitting techniques are expected to benefit greatly from Virtual Observatory access to many laboratory data currently implemented by the VESPA activity in the Europlanet program [2]. In addition, this particular method will be tested in a VO context to provide analysis on demand.

1. Extraction of band parameters

The first step in the procedure is to analyze the observed spectrum and the possible matches using the Mulțumesc method [1]. This multiscale algorithm identifies absorption features that stand out of the noise level and are detected consistently at successive scales. The analysis returns a list of possible bands with their location, width, and depth, plus several confidence parameters. One of these consists in a comparison between the retrieved band depth and a composite noise level determined from several scales; others are related to detection near the edge of the spectral domain, especially when a shoulder of the band is not complete. Since the method analyses the spectral shape, correct spectral calibration is assumed at least in relative values (Fig. 1).

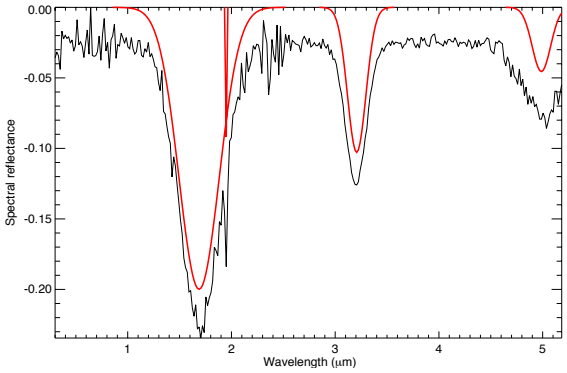

Figure 1: Simulated spectrum - overlapping Gaussians with different width and depth. Bands are reconstructed in red from estimated parameters.

A similar analysis is performed on available spectral libraries. In general, these have much higher spectral-to-noise ratio and therefore much lesser uncertainty on retrieved band characteristics. Reference libraries can be analyzed once for all, so that they are ready to use for this purpose.

2. Comparison of band parameters

Several strategies of spectral matching are being assessed and will be presented at the conference. As a general rule, a good match implies fitting the center/position of all detectable bands; the intrinsic continuum-correction involved in the multiscale analysis indeed minimizes band shifts related to continuum slopes. In contrast, band depths depend at

least on a scaling parameter, and estimated widths may vary with signal-to-noise ratio.

The global matching procedure consists in testing the location of the major bands of the reference spectrum. If all are present in the observed data, depths and widths are compared using various correlation measurements. In some cases, the confidence parameter computed in the detection step can be used as a weight in the fits.

A specific problem may arise when several bands are superimposed – in this case the algorithm may detect the bands correctly but with part of the strength deported to a different scale (common "envelop" associated to several bands, see Fig. 2), so that the correlation is not longer linear.

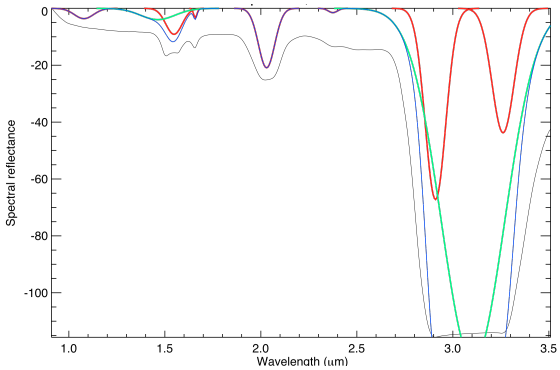

Figure 2: Ice spectrum from [3] - Individual bands are displayed in red, envelopes in green, their sum in blue.

3. Spectral match as a Virtual Observatory service

Although the band extraction algorithm is currently implemented under IDL, it can be embedded in a VO workflow and made available to process on-line data on demand. The results of the detection step will be transmitted via SAMP as a VOTable describing each detected band, for use in tools such as TOPCAT or CASSIS.

The Mulțumesc algorithm is also applied to large sets of laboratory reference data, starting with the PDS spectral library [4]. If deemed reliable, band descriptions will be distributed together with the data as an EPN-TAP data service, and will be searchable in the Virtual Observatory system set up by VESPA/Europlanet (Fig. 3). Finally, the detection tool will be enlarged to perform spectral matches with existing libraries on the basis of band characteristics.

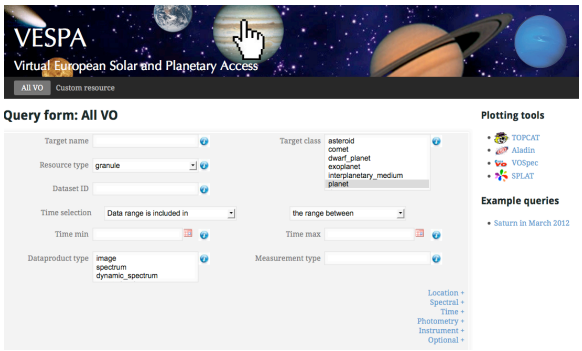

Figure 3: The VESPA user interface: http://vespa.obspm.fr

References

[1] Erard, S. (2013) Analysing spectral signatures with multiscale methods. In *EPSC2013*–520, London, UK.
[2] Erard et al (2014) Planetary Science Virtual Observatory architecture. *A&C* **7-8**, 71-80 http://arxiv.org/abs/1407.4886
[3] Mastrapa, et al (2008) Optical constants of amorphous and crystalline H_2O–ice in the near infrared from 1.1 to 2.6 µm. *Icarus* 197, 307–320.
[4] Murchie, S. et al (2007) Compact Reconnaissance Imaging Spectrometer for Mars (CRISM) on Mars Reconnaissance Orbiter (MRO). *JGR (Planets)* 112, E05S03

Acknowledgement

The Europlanet 2020 Research Infrastructure project has received funding from the European Union's Horizon 2020 research and innovation programme under grant agreement No 654208.
Additional funding was provided in France by ASOV/ CNRS-INSU & Paris Astronomical Data Centre (PADC).